Control Over Film Thickness of SnO2 Ultrathin Film Selectively Deposited on a Patterned Self-Assembled Monolayer

ARTICLE *in* LANGMUIR · NOVEMBER 2002

Impact Factor: 4.46 · DOI: 10.1021/la026158+

4 AUTHORS, INCLUDING:

Yoshitake Masuda
National Institute of Advanced Industrial Sci…
305 PUBLICATIONS **5,473** CITATIONS
SEE PROFILE

Tetsu Yonezawa
Hokkaido University
197 PUBLICATIONS **4,561** CITATIONS
SEE PROFILE

Control over Film Thickness of SnO_2 Ultrathin Film Selectively Deposited on a Patterned Self-Assembled Monolayer

Naoto Shirahata,* Yoshitake Masuda, Tetsu Yonezawa,† and Kunihito Koumoto

Department of Applied Chemistry, Graduate School of Engineering, Nagoya University, Nagoya 464-8603, Japan, and Precursory Research for Embryonic Science and Technology (PRESTO), Japan Science and Technology Corporation

Received June 29, 2002. In Final Form: September 14, 2002

This paper presents a novel process for the fabrication of site-selectively deposited tin oxide ultrathin films (<10 nm) by using molecular recognition between the precursors and the surface of the Si substrate. Using this simple technique, the film thickness of micropatterned tin oxide films was easily controlled. Patterned self-assembled monolayers, in which both hydrophilic and hydrophobic areas formed, were used as templates for the site-selective deposition of the films. Two precursors of $SnCl_4$ and $C_4H_9SnCl_3$ were selected. The films were selectively deposited on the hydrophilic regions through the liquid phase. The growth rate of the film deposited in $SnCl_4$ solution was approximately 6 times faster than that in C_4H_9-$SnCl_3$ solution. A quartz crystal microbalance measurement implied that film growth could be suppressed by the formation of hydrophobic surfaces on the growing films with increasing immersion time in C_4H_9-$SnCl_3$ solution.

1. Introduction

Ultrathin metal oxide films have attracted great interest in terms of fundamental questions in surface science. This is due to their various technological applications as photocatalysts,[1] gas-sensing devices,[2,3] insulating barriers between ferromagnetic materials in permanent magnetic random access memory (MRAM) devices,[4,5] and gate insulators in metal oxide semiconductor field effect transistors (MOSFET).[6−8] There are two types of processes involved in the production of ultrathin film, dry processes and wet processes. The former type, which employs one of two deposition methods, physical vapor deposition (PVD) or chemical vapor deposition (CVD), relies on a vacuum deposition process. The latter type of process, such as electroless deposition,[9] anodic oxidation,[10,11] and sol−gel[12] methods, is preferable as the fabrication cost is less.

More recently, great attention has been paid to the production of micro- and nanoelectronic devices integrated on a chip.[13] For this purpose, a variety of lithography techniques have been investigated such as X-ray/electron-beam lithography and photolithography,[14] microcontact printing,[15,16] wet etching,[17] ink-jet printing,[18] embossing,[19,20] slip-pressing,[21] charge-based printing,[22] micromolding,[23] and cold welding.[24] Among these techniques, there has been a growing interest in forming a metal oxide thin film by site-selective deposition on a patterned self-assembled monolayer (SAM) as a simple low-cost fabrication process.[25−27] On the basis of this approach, Masuda et al.[28,29] have reported a fabrication technique which permits the micropatterned metal oxide thin film to be site-selectively deposited on a silanol region in the

* To whom correspondence should be addressed. Tel: +81-52-789-3329. Fax: +81-52-789-3201. E-mail: n_shirahata@nucc.cc.nagoya-u.ac.jp.

† Precursory Research for Embryonic Science and Technology (PRESTO), Japan Science and Technology Corp.

(1) Ichinose, I.; Kawakami, T.; Kunitake, T. *Adv. Mater.* **1998**, *10*, 535−539.
(2) Olvera, M. de la L.; Asomoza, R. *Sens. Actuators* **1997**, *B45*, 49−53.
(3) Mizsei, J.; Pirttiaho, L.; Karppinen, M.; Lantto, V. *Sens. Actuators* **2000**, *B65*, 195−198.
(4) Moodera, S.; Kinder, L. R.; Wong, T. M.; Meservey, R. *Phys. Rev. Lett.* **1998**, *75*, 3273−3276.
(5) Jeliazova, Y.; Franchy, R. *Appl. Surf. Sci.* **2002**, *187*, 51−59.
(6) Campbell, S. A.; Kim, H.-S.; Gilmer, D. C.; He, B.; Ma, T.; Gladfelter, W. L. *IBM J. Res. Dev.* **1999**, *43*, 383−392.
(7) Eisenbeiser, K.; Finder, J. M.; Yu, Z.; Ramdani, J.; Curless, J. A.; Hallmark, J. A.; Droopad, R.; Ooms, W. J.; Salem, L.; Bradshaw, S.; Overgaard, C. D. *Appl. Phys. Lett.* **2000**, *76*, 1324−1326.
(8) Wilk, G.; Wallace, R. *Appl. Phys. Lett.* **1999**, *74*, 2854−2856.
(9) Saito, N.; Haneda, H.; Seo, W. S.; Koumoto, K. *Langmuir* **2001**, *17*, 1461−1469.
(10) Grecea, M.; Rotaru, C.; Nastase, N.; Graciun, G. *J. Mol. Struct.* **1999**, *480−481*, 607−610.
(11) Richardson, T. J.; Slack, J. L.; Rubin, M. D. *Electrochim. Acta* **2001**, *46*, 2281−2284.
(12) Hosoya, Y.; Suga, T.; Yanagawa, T.; Kurosawa, Y. *J. Appl. Phys.* **1997**, *81*, 1475−1480.
(13) Hagleitner, C.; Hierlemann, A.; Lange, D.; Kummer, A.; Brand, O.; Baltes, H. *Nature* **2001**, *414*, 293−296.
(14) Cho, Y. R.; Lee, J. H.; Song, Y. H.; Kang, Y. S.; Hwang, C. S.; Jung, M. Y.; Kim, D. H.; Lee, S. K.; Uhm, H. S.; Cho, K. I. *Mater. Sci. Eng.* **2001**, *B79*, 128−132.
(15) Jeon, N. L.; Clem, P. G.; Nuzzo, R. G.; Payne, D. A. *J. Mater. Res.* **1995**, *10*, 2996−2999.
(16) Aizenberg, J.; Braun, P. V.; Wiltzius, P. *Phys. Rev. Lett.* **2000**, *84*, 2997−3000.
(17) Nashimoto, K.; Haga, K.; Watanabe, M.; Nakamura, S.; Osakabe, E. *Appl. Phys. Lett.* **1999**, *75*, 1054−1056.
(18) Motto, M.; Song, J. H.; Evans, J. R. G. *J. Am. Ceram. Soc.* **1999**, *82* 1653−1658.
(19) Stutzmann, N.; Tervoort, T. A.; Bastiaansen, C.; Feldmann, K.; Smith, P. *Adv. Mater.* **2000**, *12*, 557−562.
(20) Matsuda, A.; Matsuno, Y.; Tasumisago, M.; Minami, T. *J. Am. Ceram. Soc.* **1998**, *81*, 2849−2852.
(21) Bauer, W.; Ritzhaupt-Kleissl, H. J.; Hausselt, J. *Ceram. Int.* **1999**, *25*, 201−205.
(22) Jacobs, H. O.; Whitesides, G. M. *Science* **2001**, *291*, 1763−1766.
(23) Kim, E.; Xia, Y.; Whitesides, G. M. *Nature* **1995**, *376*, 581−584.
(24) Kim, C.; Burrows, P. E.; Forrest, S. R. *Science* **2000**, *288*, 831−833.
(25) Shin, H.; Collins, R. J.; De Guire, M. R.; Heuer, A. H. *Acta Mater.* **1998**, *46*, 801−805.
(26) Koumoto, K.; Seo, S.; Sugiyama, T.; Seo, W. S.; Dressick, W. J. *Chem. Mater.* **1999**, *11*, 2305−2309.
(27) Saito, N.; Ohashi, N.; Haneda, H.; Koumoto, K. *Adv. Mater.* **2002**, *14*, 418−421.
(28) Masuda, Y.; Seo, W. S.; Koumoto, K. *Thin Solid Films* **2001**, *382*, 153−157.
(29) Masuda, Y.; Jinbo, Y.; Yonezawa, Y.; Koumoto, K. *Chem. Mater.* **2002**, *14*, 1236−1241.

10.1021/la026158+ CCC: $22.00
Published on Web 11/20/2002

patterned octadecyltrichlorosilane (OTS) SAM. This technique, which is a buildup type of process, can be expected to result in a smart low-cost fabrication process where the functional metal oxide thin films are site-selectively deposited on the substrate. However, detailed research that considers the control of thin film thickness has not been conducted.

Chemical etching of SnO_2 is very difficult due to its high chemical durability. However, SnO_2 has high levels of optical transparency, chemical durability, and gas sensitivity, and the starting materials are inexpensive. Therefore, site-selectively deposited SnO_2 may, if available, be a very attractive material for application to micro- and nanoelectronic devices. An ultrathin SnO_2 film is required for gas-sensing devices, since gas sensitivity increases drastically with decreased film thickness.[2] Several reports have already been published on the patterning of SnO_2 thin films. Kikuta et al.[30] have reported on the photoreaction of tin precursors following the addition of diethanolamine or phenyldiethanolamine. The fine patterning of the precursor film was achieved via irradiation using an ultrahigh-pressure mercury lamp fitted with a photomask. Tamai et al.[31] have reported on the patterning of SnO_2 thin films with film thicknesses from 0.15 to 1 μm. This was achieved by lithographic photoirradiation, followed by pyrolysis of a tin analogue of poly(4-((trimethylsilyl)methyl)styrene) film. Tadanaga et al.[32] have reported fine patterned SnO_2 thin films, with thicknesses of about 100 nm. These have been produced through UV irradiation, using a high-pressure mercury lamp, plus heat treatment of precursor films on the substrate. To our knowledge, none of the techniques have been reported to achieve the successful selective deposition of micropatterned tin oxide ultrathin film on a patterned SAM.

In the present study, we suggest a smart fabrication technique for a site-selectively deposited and micropatterned SnO_2 ultrathin film utilizing molecular recognition between the precursors and the surface of the Si substrate.

2. Experimental Procedure

2.1. Patterned SAM Preparation. A P-type Si (100) wafer with a resistivity in the range of 5−10 Ω cm was used as the substrate. The substrates were first degreased ultrasonically in toluene, ethanol, and deionized water (resistivity = 18.3 MΩ). They were then exposed for 2 h to UV light (184.9 nm) with Hg lamps in ambient air in order to remove any contamination adsorbed on their surfaces. An OTS-SAM substrate was prepared by immersing the cleaned Si substrate in an anhydrous toluene (99.8%, water < 0.002%, Aldrich) solution containing 1.0 vol % OTS at room temperature for 5 min under a N_2 atmosphere. After immersion, the OTS-SAM substrate was carefully rinsed several times in new toluene and then heated at 120 °C for 5 min in order to polymerize the OTS. The patterned OTS SAM was fabricated by UV irradiation for 2 h in ambient air through a photomask. A copper grid mesh, normally used for transmission electron microscopy, was employed as a photomask. The UV-irradiated regions became hydrophilic regions as a result of Si−OH group formation (silanol region), while the nonirradiated area remained unchanged, that is, it was composed of hydrophobic octadecyl groups (methyl region), which gave rise to patterned OTS SAMs. To check whether SAM formation and functional group changes had occurred, water drop contact angles were measured for the irradiated and nonirradiated areas. Initially deposited OTS SAMs had water contact angles from 96 to 102°. The UV-irradiated area, however, was saturated (water contact angles of <5°).

2.2. Formation of Hydrated Tin Oxide Thin Film and Heat Treatment. Two kinds of precursors were selected as starting materials: tin(IV) chloride (TC) and butyl tin trichloride (BTT). The patterned OTS-SAM substrates were immersed in an anhydrous toluene solution containing these precursors (0.0045 and 0.05 mol/L) at room temperature for immersion times from 1 to 40 min under a N_2 atmosphere. After the desired immersion time, the residual solvent on the surface of the samples was immediately rinsed away using new toluene and then the samples were wiped off. Because of the extreme sensitivity of the starting materials to H_2O molecules, reactors with the same amount of H_2O content were used for depositing the films in TC and BTT solutions. The as-deposited films were heated and held at temperatures ranging from 100 to 600 °C for 3 h in ambient air in order to obtain both amorphous tin oxide and crystallized films. The heating rate was 10 °C/min.

2.3. Characterization. Thin-film X-ray diffraction (XRD, Rigaku, RU200), with a 5° incident angle using Cu Kα radiation with a Ni filter and graphite monochromator (40 kV, 30 mA), was used to detect the crystallized phase in the films before and after heat treatment. The scanning speed was 1°/min, and the scanning range was from 5 to 100°. The functional groups in the films were detected by a Fourier transform infrared spectrometer (FT-IR; Hitachi, 270-30) under a N_2 stream. A scanning electron microscope (SEM; Hitachi, S-3000N) operating at an accelerating voltage of 20 kV was used to observe the surface morphologies of the selectively deposited films on the patterned OTS SAMs. X-ray photoelectron spectroscopy (XPS; Mg Kα) operated at 15 kV and 18 mA under high-vacuum (1.0×10^{-10} Pa) conditions in order to investigate the Cl 2p region. The spectrum was corrected for possible surface charging with respect to the C 1s line, which is normally attributed to the contamination adsorbed at the surface of the film and peaked at 284.6 eV. Film thickness and surface morphology were measured using an atomic force microscope (AFM; Nanoscope E, Digital Instruments). The film thicknesses were measured, before and after heat treatment, in the observed areas including several micropatterns of the film. Surface roughness, as evaluated by root mean square (RMS), can be expressed as

$$\text{RMS (standard deviation)} = [\sum_i (Z_i - Z_{ave})^2/n]^{1/2} \quad (1)$$

where Z_i is the height at point i, Z_{ave} is the average of Z, and n is the number of data points. Thermogravimetry analysis (TG; Rigaku, TG8120) was conducted to measure weight changes in the hydrolyzed BTT samples within a temperature range from 23 to 600 °C under ambient air conditions. The heating rate was 10 °C/min. The hydrolyzed BTT samples for TG analysis were prepared by hydrolyzing BTT in an aqueous solution at room temperature. A quartz crystal microbalance (QCM; QCA917, Seiko), is an ultrasensitive weighing device and can determine mass loading below 1 ng by measuring the resonant frequency.[46] The QCM was used to analyze the growth behavior of tin hydroxide films at the surfaces of the silanol and methyl regions in BTT solution (0.05 mol/L). The QCM was also tried in order to discover the difference in film growth rates between the silanol regions in TC and BTT (0.05 mol/L) solutions. 2-Mercaptoethanol was employed to form the silanol region (OH SAM) on the gold electrode of the quartz oscillator surface.[33] The methyl region (CH_3 SAM) was prepared by the formation of OTS on the OH SAM. In this report, the abbreviations "OH SAM" and "CH_3 SAM" were used to distinguish between the silanol and methyl regions that formed on the gold electrode of quartz oscillator surfaces on the respective SiO_2/Si substrates.

3. Results

3.1. Film Growth Rates in TC and BTT Solutions. Figure 1a shows the time dependence of the as-deposited film thickness obtained in TC and BTT solutions. Figure 1b shows the time dependence of crystallized ultrathin SnO_2 film thickness when deposited in a BTT solution

(30) Kikuta, K.; Suzumori, K.; Takagi, K.; Hirano, S. *J. Am. Ceram. Soc.* **2002**, *82*, 2263−2265.
(31) Tamai, T.; Ichinose, N.; Kawanishi, S.; Nishii, M.; Sasuga, T.; Hashida, I.; Mizuno, K. *Chem. Mater.* **1997**, *9*, 2674−2675.
(32) Tadanaga, K.; Owan, T.; Morinaga, J.; Urbanek, S.; Minami, T. *J. Sol.-Gel Sci. Technol.* **2000**, *19*, 791−794.
(33) Raj, C. R.; Ohsaka, T. *Bioelectrochemistry* **2001**, *53*, 251−256.

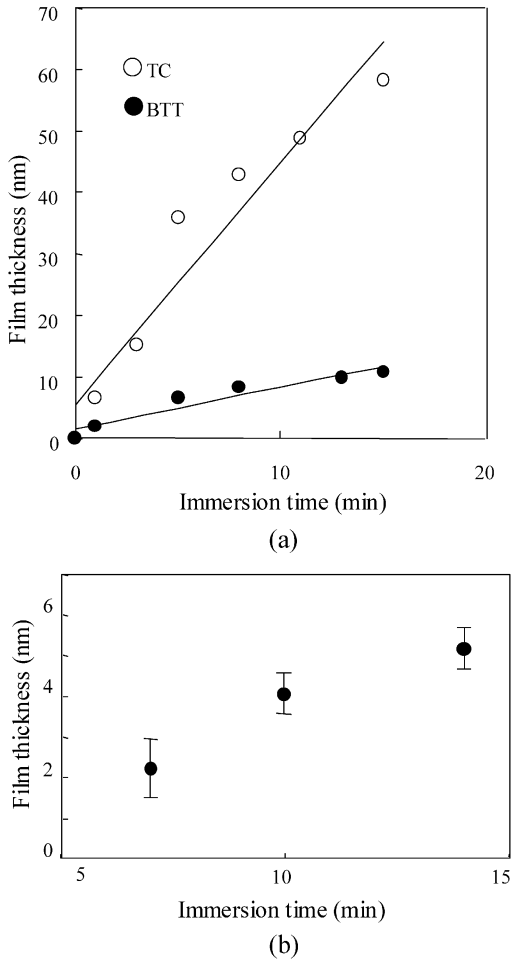

Figure 1. (a) Immersion time dependence of the thickness of tin hydroxide thin films deposited in TC and BTT (0.0045 mol/L) solutions. The equations obtained by curve fitting are as follows: TC, $d = 3.93T + 5.59$ ($R^2 = 0.92$); BTT, $d = 0.68T + 1.49$ ($R^2 = 0.92$). (b) Immersion time dependence of the thickness of the ultrathin SnO_2 films, which were obtained by heat treatment at 600 °C for 3 h under ambient air. All films were obtained in BTT solutions with the concentration of 0.05 mol/L.

(0.05 mol/L), heated at 600 °C for 3 h under ambient air conditions. Linear relationships resulting from the fitted curve were kept for both TC and BTT, as shown in Figure 1a. The fitted equations are shown in the Figure 1 caption. The R^2 values indicate the goodness of fit for these curves. The film grew rapidly and selectively on the silanol region as soon as the patterned OTS-SAM substrate was immersed in the TC solution. In contrast, the growth rate of as-deposited film in the BTT solution was very low. The most intriguing aspect of this was that the film growth rate in the TC solution (about 4.0 nm/min) was about 6 times higher than that in a BTT solution (about 0.7 nm/min). Growth rates generally increase with solution concentration, and so in the case of the TC solution, it is difficult to control the ultrathin film thickness (<10 nm) due to its high growth rate, even in very dilute solutions of 0.0045 mol/L. In contrast, using the BTT solutions, it was easy to obtain ultrathin film micropatterns with film thicknesses ranging from 2 to 5 nm, as shown in Figure 1b. Figure 2 shows RMS changes to the surfaces of as-deposited thin films obtained in TC and BTT solutions as a function of immersion time. The RMS values and their standard deviations gradually decrease with an increase in film thickness in both as-deposited thin films. In particular, the RMS values of the thin films deposited in

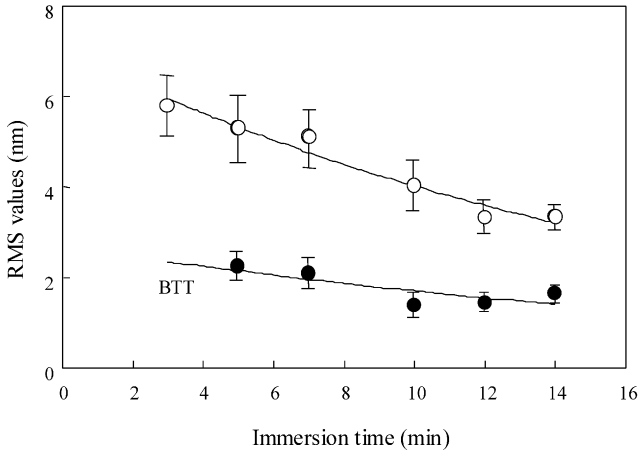

Figure 2. The RMS changes of the patterned thin films deposited in TC and BTT (0.05 mol/L) solutions with immersion time under a N_2 atmosphere.

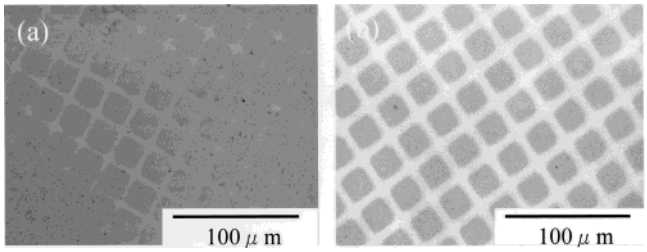

Figure 3. SEM images showing the micropatterned thin films selectively deposited in (a) TC (for 10 min) and (b) BTT (for 14 min) solutions in a N_2 atmosphere.

a BTT solution are much lower than those of films deposited in a TC solution. As shown in Figures 1 and 2, the films, particularly those generated in BTT solutions, grew slowly and maintained low RMS values from the initial growth point. The TC solutions became slightly cloudy with increasing immersion time, because of the precipitates formed in the solutions. Indeed, a large amount of precipitates was observed on all sides of the reactor vessel after the desired immersion time in TC solution, while in the case of the BTT solution, few precipitates could be verified by AFM observation.

3.2. Selective Deposition and Micropatterning. Figure 3 illustrates SEM images showing micropatterned thin films selectively deposited on silanol regions in (a) TC and (b) BTT solutions (0.05 M) under a N_2 atmosphere, respectively. In both images, the white and black contrasts represent the methyl region and the film grown on the silanol region, respectively, as discussed later in detail. As shown in the SEM images, it was easy to obtain a high-resolution pattern of the film without chlorine atoms analyzable by XPS. However, the speckles shown by the black contrast in image a were observed in the methyl region of the sample obtained in TC solution. This means that the film growth occurred in the methyl region. SEM images are used in Figure 4 to show the morphology of the films deposited on the patterned OTS-SAM substrates in a BTT (0.05 mol/L) solution as a function of time. The film began to grow at 3 min after immersion and continued to grow only on the silanol regions between 3 and 14 min. Serious difficulty was, however, encountered in the observation of the high-resolution pattern of the film after the immersion time of 16 min, because of the new appearance of two types of growth configurations. One was the film growth on both silanol and methyl regions, as shown in Figure 4e,f. The other was a lateral growth to the surface normal. Indeed, it was revealed that the

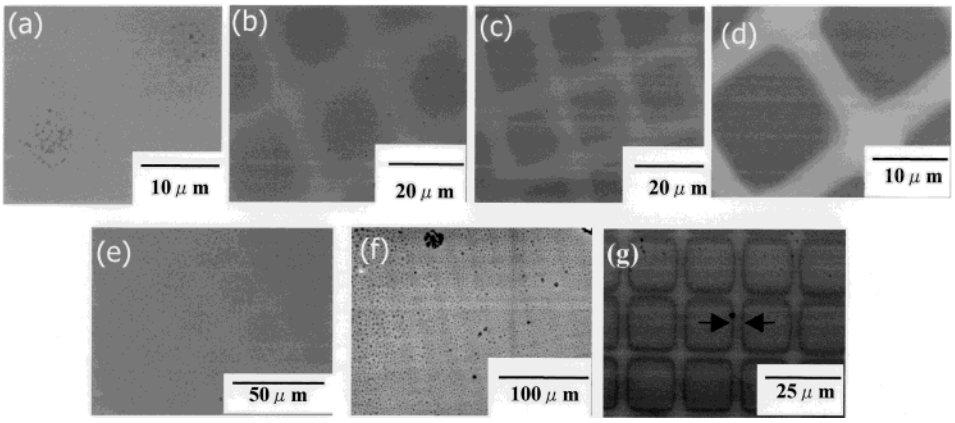

Figure 4. SEM images showing the immersion time dependence of the growth direction and regions of tin hydroxide thin films, deposited in BTT solution (0.05 mol/L), on the patterned SAM. The patterned films were obtained for the immersion times of (a) 5 min, (b) 7 min, (c) 10 min, (d) 14 min, (e) 16 min, (f) 18 min, and (g) 18 min, respectively. The arrows in the image of (g) show the growth directions of the films changing from a unidirectional growth to an isotropic one.

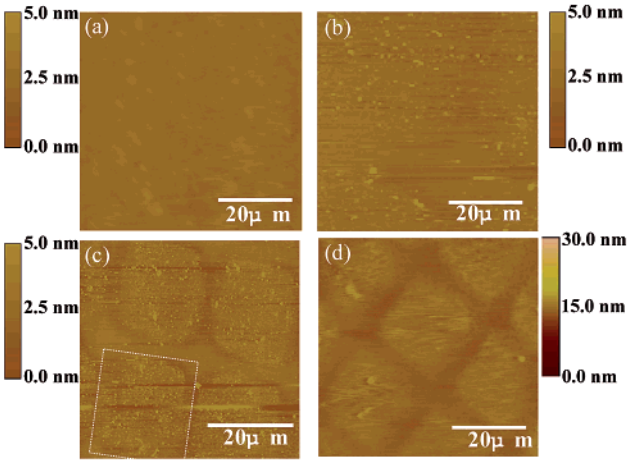

Figure 5. AFM images of the micropatterned tin hydroxide thin films, selectively deposited on silanol regions in the patterned OTS-SAMs in BTT solutions (0.05 mol/L), with immersion times of (a) 0 min, (b) 3 min, (c) 5 min, and (d) 14 min. In the images, the dotted lines show the silanol regions in the patterned OTS-SAMs.

line width of the methyl region narrowed, as indicated by the arrows in Figure 4g. It was impossible to observe the thin film micropatterns after the 20 min immersion time. Figure 5 illustrates the AFM images indicating the growth process of the thin film micropatterns in a BTT solution (0.05 mol/L) with immersion time. Film growth began to occur within the silanol region; however, none of the micropatterns in the sample were observable for the immersion time of 3 min when comparing image a with image b. Since the thin film only imperfectly covered the silanol region, dense, almost perfect micropatterns were observed in the sample only after an immersion time of 5 min. This is indicated by the dotted line in image c. Dense, perfect micropatterns were observed when immersion times ranged from 7 to 14 min, as shown in image d. It was also verified that film thickness also increased with time and that film growth occurred selectively on silanol regions in the patterned OTS-SAM substrate.

Figure 6 shows SEM images indicating the effect of heat treatment on micropattern resolution. None of the resolution changes were observed before and after heat treatment, as shown in Figure 6. After crystallization, film thickness was approximately halved from 12.6 ± 1.06 nm to 5.17 ± 1.00 nm. The RMS value for the surface of the heated sample was measured to be 1.27 ± 0.46 nm, which was as low as that for the as-deposited film surface.

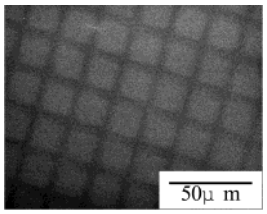

Figure 6. SEM image showing the micropatterned thin film, which was the same sample shown in Figure 4d, crystallized at 600 °C for 3 h in ambient air.

3.3. Characterization of Films. Thin film XRD patterns revealed that the crystalline phase occurred in as-deposited films and in films fired below 600 °C; however, crystalline SnO_2 with the cassiterite type structure was found in the film fired at 600 °C for 3 h under ambient air. Figure 7 shows FT-IR spectra of the as-deposited thin film and annealed films produced in BTT solutions, for annealed temperatures ranging from 100 to 600 °C. A peak (see Figure 7a) at 3370 cm^{-1} was observed in the as-deposited film. In general, the bands observed at around 3400 cm^{-1} were assigned to the hydroxyl bands.[34] For qualitative analysis of this peak, three kinds of hydroxyl bands were considered: Si−OH, Sn−OH, and physisorbed water. It was reasonable that the peak corresponded to the vibration band, which is attributable to Sn−OH appearing at around 3400 cm^{-1},[35] because the Si−OH vibration band at 960 cm^{-1} and the OH vibration can be ascribed to physisorbed water at 3450 cm^{-1}.[35] The Sn−OH vibration band was not observable in the spectrum above 200 °C. In Figure 7b, three kinds of peaks were observed at 560, 615, and 660−680 cm^{-1}. Both of the bands appearing at 560 and 660−680 cm^{-1} were attributed to the vibration of O−Sn−O groups.[36−38] Pettinari et al.[39] reported that the band at around 610 cm^{-1} has been attributed to the stretching band of the Sn−C bond in di-*n*-butyl tin dichloride. The peak observed at 615 cm^{-1} in as-deposited film corresponded to the stretching band

(34) Pei, Z.-F.; Ponec, V. *Appl. Surf. Sci.* **1996**, *103*, 171−182.
(35) Salas, P.; Hernández, J. G.; Montoya, J. A.; Navarrete, J.; Salmones, J.; Schifter, I.; Morales, J. *J. Mol. Catal. A: Chem.* **1997**, *123*, 149−154.
(36) Epifani, M.; Alvisi, M.; Mirenghi, L.; Leo, G.; Siciliano, P.; Vasanelli, L. *J. Am. Ceram. Soc.* **2001**, *84*, 48−54.
(37) Jiménez, V. M.; Caballero, A.; Fernandez, A.; Espiós, J. P.; Ocaña, M.; González-Elipe, A. R. *Solid State Ionics* **1999**, *116*, 117−127.
(38) Huang, H.; Kelder, E. M.; Chen, L.; Schoonman, J. *Solid State Ionics* **1999**, *120*, 205−210.
(39) Pettinari, C.; Marchetti, F.; Cingolani, A.; Bartolini, S. *Polyhedron* **1996**, *15*, 1263−1276.

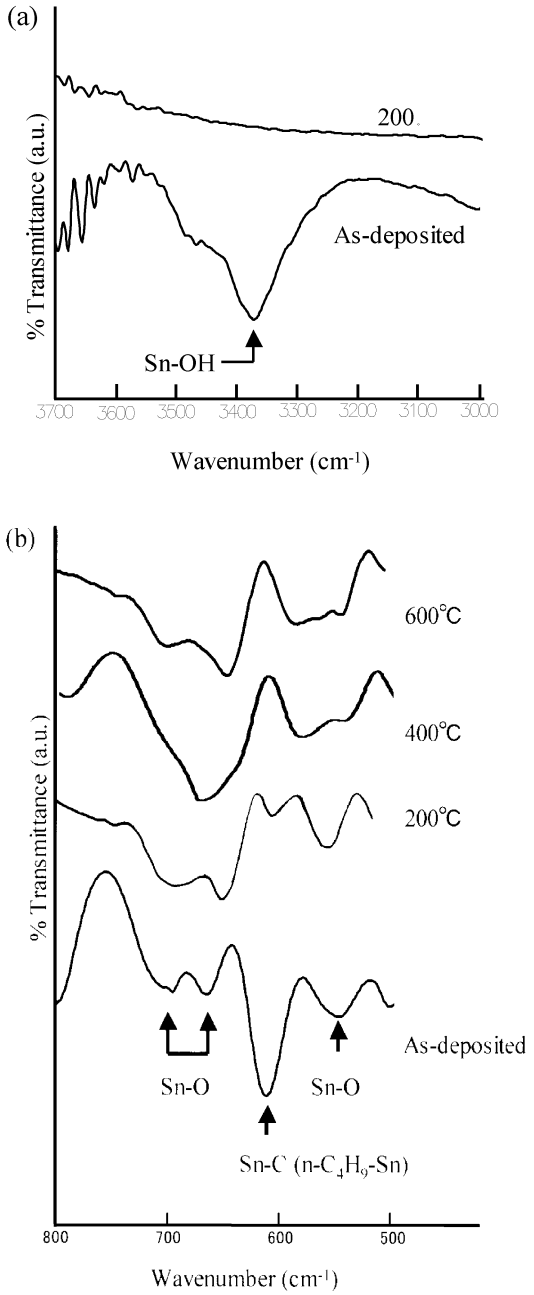

Figure 7. FT-IR spectra of as-deposited thin film and heated ones, obtained in a BTT solution, in the temperature range from 100 to 600 °C in air: (a) 3000−3700 cm^{-1} and (b) 500−800 cm^{-1}.

of Sn−C. The Sn−C stretching band intensity decreased with temperature and then disappeared at 400 °C. The C−H stretching, which has generally been observed at 2900−2950 cm^{-1},[40] was also detected in as-deposited film, and its peak intensity decreased with temperature. It finally disappeared above 400 °C. From the above results shown in Figure 7, amorphous SnO_2 thin films are obtained above 400 °C and crystalline thin films are developed above 600 °C. Figure 8 shows a TG curve of the hydrolyzed BTT sample (n-$C_4H_9Sn(OH)_3$). The TG result showed a total weight loss of 35.86% at 400 °C, which was divided into separate weight losses of 10.93% at 200 °C and 24.93% at 400 °C. From the FT-IR results shown in Figure 7, the thermal compositional changes of as-deposited thin film were as follows: n-$C_4H_9Sn(OH)_3$ (as-deposited) → n-$C_4H_9SnO_{1.5}$ (200 °C) → SnO_2 (400 °C). Thermogravimetric changes, based on the FT-IR results, were calculated to be 11.90 wt % at 200 °C and 33.57 wt % at 400 °C. As the calculated values corresponded to the experimental values within experimental error, it is reasonable

(40) Chao, C. C.; Tsai, D. S. *J. Membr. Sci.* **2001**, *192*, 209−216.

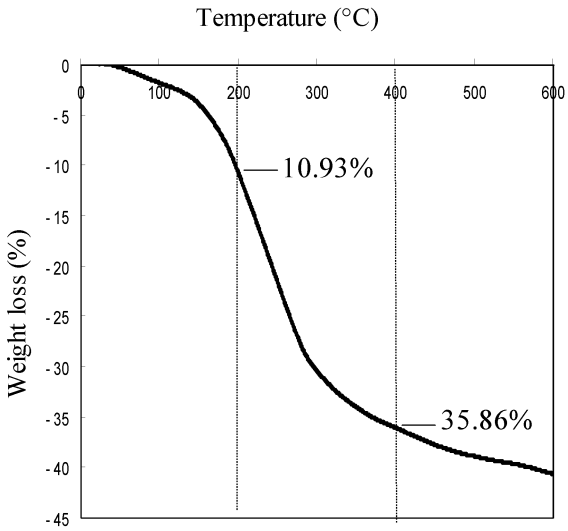

Figure 8. TG curve of the hydrolyzed BTT sample, which was precipitated in an aqueous solution including the BTT precursor in the temperature range from 23 to 600 °C under ambient air. The heating rate was 10 °C/min.

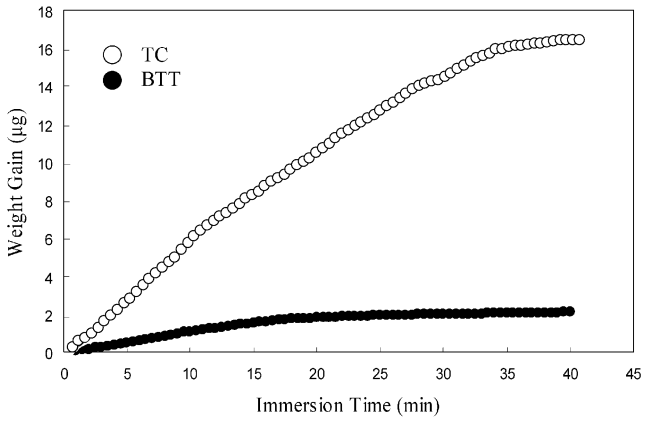

Figure 9. Time dependence of QCM weight gain by deposited film on OH SAMs in an anhydrous toluene solution containing TC and BTT precursors (0.05 mol/L) under a N_2 atmosphere.

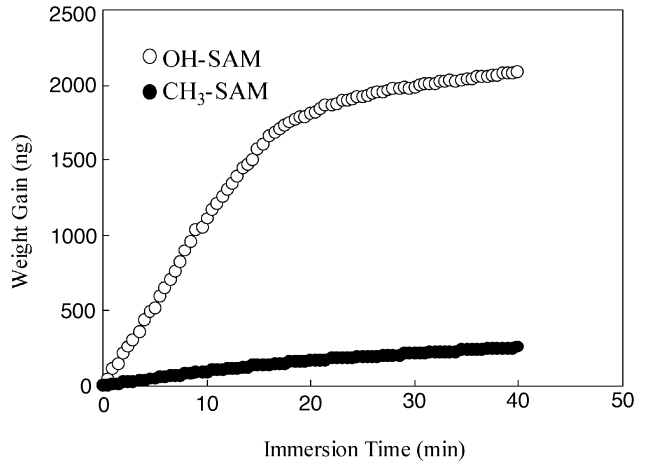

Figure 10. Time dependence of QCM weight gain by deposited film on OH and CH_3 SAMs in an anhydrous toluene solution containing BTT precursor (0.05 M) under a N_2 atmosphere.

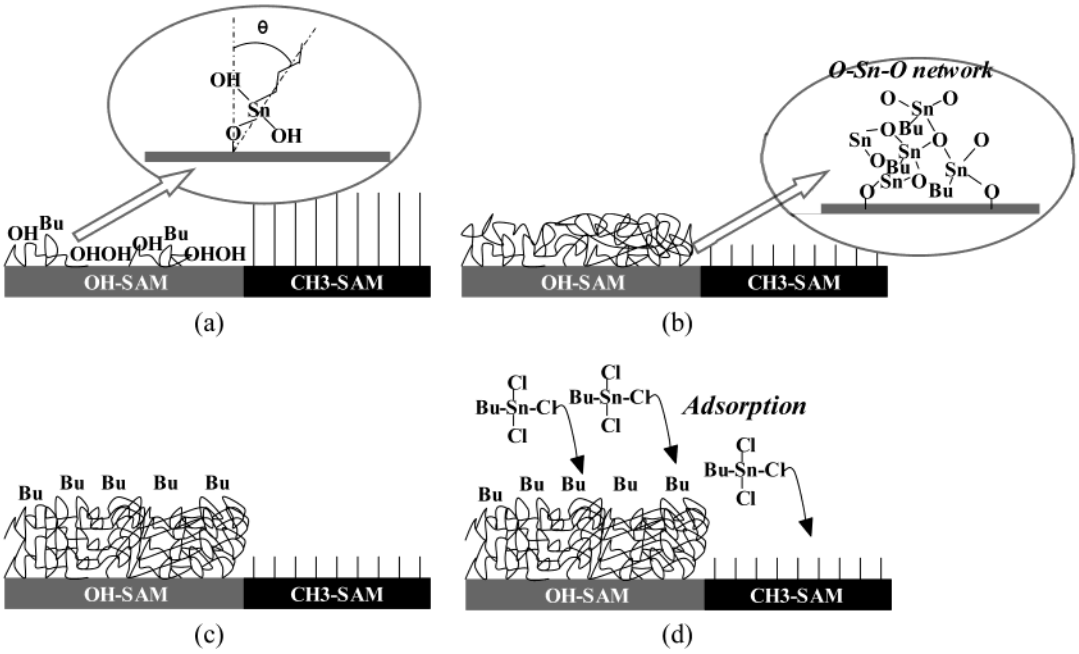

Figure 11. Illustrations for the growth process of tin hydroxide thin films in a BTT solution with immersion time.

to accept the above-mentioned compositional change of the as-deposited film.

4. Discussion

It is generally known that the reactivity of silicon chloride with H_2O molecules is highest among silicon alkoxide and the other silicon halides: Si−Cl > Si−F > Si−OCH_3 > Si−OC_2H_5.[41,42] Masuda et al. tried to form micropatterns of TiO_2 thin films on OTS SAMs using titanium tetrachloride, titanium dichloride diethoxide, and titanium tetraethoxide.[29] This report has demonstrated that chlorine atoms in the starting precursors are indispensable when fabricating a film micropattern because of their high reactivity with H_2O molecules. In fact, efforts to form a micropattern of tin hydroxide film in the current study by immersing the patterned OTS-SAM substrate into the aqueous solution containing SnF_2 failed. Accordingly, it is considered that tin hydroxide films selectively deposited onto silanol regions in TC and BTT solutions through hydrolysis with H_2O molecules adsorbed on silanol regions. Figure 9 shows the weight gain on OH SAMs as a function of immersion time in TC and BTT solutions (0.05 mol/L). A similar starting point in weight gain was observed with TC and BTT solutions. The growth rate in the TC solution (0.584 μg/min, $R^2 > 0.99$) was estimated to be about 6 times faster than that in the BTT solution (0.107 μg/min, $R^2 > 0.99$) with immersion times ranging from 0 to 15 min. This behavior corresponded approximately to the results shown in Figure 1. It is likely that the different growth rates in each solution closely relate to the film growth processes, as discussed later. First, we discuss the film growth process in the TC solution. The maximum weight gain rate of ~0.618 μg/min was estimated at ~33 min, and this continued to decrease and finally became constant after sufficiently long immersion times in a TC solution. This growth kinetics can be considered to result from film growth involving both heterogeneous nucleation and deposition of nanosized primary particles formed in the TC solution. This consideration is supported by the experimental fact that a number of homogeneous precipitates were observed in the TC solution (see section 3.1). Because of their small size, these particles would have a greater tendency to aggregate. As the solution became unstable with immersion time, the number of the primary particles decreased, causing a lower aggregation rate that decreased the number density of the precipitates settled onto the substrate. As a result, after 33 min, film growth should progress on the existing precipitates and grown film by hydrolysis of the TC precursor, based on a general heterogeneous nucleation mechanism. For films generated in BTT solutions, the rate of weight gain varied with time and in the interval from 0 to 33 min reached the maximum rate of 0.113 μg/min. This rate was very much lower than the rate in the TC solution. This difference could be due to the difference in reactivity of TC and BTT precursors with H_2O molecules in each solution. BTT, in solution, has a low ability to form tin hydroxide particles, since the butyl chain in the BTT precursor may sterically hinder hydrolysis and condensation in its solution. Therefore, film growth can heterogeneously occur by hydrolysis on the substrate, without the formation of nanosized primary particles in the BTT solution.

The high reactivity of TC with H_2O molecules may have an adverse effect on the formation of metal oxide ultrathin film micropatterns since, as shown in Figure 1a, the film growth rate is too high even in very dilute solution. In addition, large amounts of tin hydroxide particles, which would be formed by hydrolysis and condensation in the TC solution, would settle not only on the silanol but also on the methyl regions. A particle settled on the methyl region may become a new site of origin for film growth, as shown in Figure 3a, and furthermore, it could bring about the formation of a rough surface within a level of several nanometers, as shown in Figure 2. In contrast, BTT would be favorable for smooth-surfaced ultrathin film formation, due to its low growth rate (see Figure 1). Figure 10 demonstrates the dependence of weight gain on immersion time for OH and CH_3 SAMs in a BTT solution (0.05 mol/L). The weight gain behavior can be described

(41) Mehrotra, R. C.; Gupta, V. D.; Srivastiva, G. *Rev. Silicon, Germanium, Tin Lead Compd.* **1975**, *1*, 299.
(42) Voronkov, M. G.; Mileshevich, V. P.; Yuzhelevski, Yu. A. *The Siloxane Bond*; Plenum: New York, 1977.

as having two stages. The first stage shows rapid growth for immersion times ranging from 0 to 15 min, and the second stage is slow growth for immersion times ranging from 15 to 40 min. Interestingly, the time at which the growth kinetics changes in BTT solutions clearly differed from that in TC solutions. From the viewpoint of growth kinetics, the film growth behavior in the second stage seems to be similar to that in the CH_3 SAM, because the growth rate of 17.03 ng/min ($R^2 = 0.90$) on the OH SAM in the second stage gradually approaches that of 6.167 ng/min ($R^2 = 0.97$) on the CH_3 SAM for immersion times ranging from 0 to 40 min as in the first stage. In addition, the film growth occurred on both OH and CH_3 regions after 15 min, as shown in Figure 4e,f.

From these facts, the film growth mechanisms in the BTT solution can be considered as follows. We believe that since the BTT precursor is similar to the alkyltrichlorosilane SAM (for example, the OTS SAM) in molecular structure, the BTT precursor would bond by hydrolysis to the silanol region on the Si substrate to form a monolayer. It is well-known that chain length in the alkyltrichlorosilane SAM has an effect on monolayer quality.[43] For shorter chain lengths (alkyl chain length $n < 6$), the water contact angle decreases relative to that for longer chain lengths, indicating that the shorter chains are not as well packed on the substrate.[44] The behavior of the SAM, as mentioned above, would suggest that the tilt angles of the alkyl chains to the surface normal are higher due to the shortening of the alkyl chain length in the SAM. We therefore believe that tin hydroxide precursors would adsorb and bond by hydrolysis to the silanols to form the monolayer, with the higher tilt angles ($\theta \gg 0°$) to the surface normal, as shown in Figure 11a. The hydrolyzed BTT precursors would then bond to the silanols on the growing film by forming Sn−O−Sn networks by hydrolysis in the first stage, as shown in Figure 11b. This consideration corresponds to the growth behavior observed in Figure 4a−d. However, hydrophobicity at the surface of the growing film would increase with increased film thickness. Eventually the hydrophobic surface would mainly cover the surface of the growing film, as shown in Figure 11c. After formation of the hydrophobic surface, it is reasonable to assume that no more regions for the selective deposition of film would be found in the substrate. Therefore, film growth by hydrolysis must be restricted. It should occur on both silanol and methyl regions in the patterned substrate by nonselective adsorption of the precursors to each region, as shown in Figure 11d. The drastic change in weight gain rate, as shown in Figure 10, implies that the growth process of the films changes from the hydrolysis process to the adsorption process at the critical immersion time of 15 min. In fact, the water contact angle of the silanol region was verified to be almost equal to that of the methyl region immersed in a BTT solution (0.05 mol/L) for 15 min. This consideration coincides with the experimental facts as shown in Figures 4 and 10. In contrast, since no hydrophobic surfaces appeared within the immersion time, the thicker film ($d > 10$ nm) would appear to grow selectively on the silanol region in the TC solution (see Figures 1 and 9). Two mechanisms can be considered as explanations for the destruction of micropatterns as shown in Figure 4f,g. One is film growth on both the silanol and methyl regions, as mentioned above (Figure 4f); the other is film growth within the immersion time that is parallel to the surface (Figure 4g) as observed frequently in the samples after the immersion time of 16 min.

As mentioned above, film thickness was approximately halved after crystallization at 600 °C for 3 h under ambient air. In contrast, none of the resolution changes were observed in the micropatterns before and after crystallization, according to comparison of Figures 3 and 6. AFM observation also verified that patterned film shrinkage occurred only in a direction parallel to the growth. These experimental facts mean that the film shrinks only in one direction of surface normal through the heat treatment. There are two reasons why film thickness was approximately halved after crystallization. One is thermal decomposition of $Sn(OH)_4$ to SnO_2 accompanying the shrinkage of about 25 vol %,[45] and the other is the removal of butyl chains, accompanying the shrinkage change from $BuSnO_{1.5}$ to SnO_2. The patterned film shrinkage mechanism due to temperature would be accomplished by their synergistic effects. In addition, judging from the differences of dissociation energies between Sn−Bu (46.7 kcal/mol) and Sn−O (131 kcal/mol), it may be possible to remove only the carbon source from the film. However, this consideration holds under the specific condition that the deposited films are fully dense. To clarify the ideal and/or calculated volume shrinkage accompanying the removal of butyl chains, some experimental information, such as experimental tilt angles of hydrolyzed BTT precursors to the surface normal and quantification analysis of the packed density of the precursors, will be required.

5. Conclusion

It was found that a selectively deposited, micropatterned SnO_2 ultrathin film could be formed using a simple, smart solution system and an associated low-cost process. Tin oxide films with a variety of thicknesses were selectively deposited on silanol regions, using patterned OTS-SAM substrates prepared by photolithography in ambient air, using TC and BTT starting precursors. The film growth rate in TC solution was about 6 times faster than that in BTT. Amorphous tin oxide film was obtained by heat treatment in ambient air at temperatures above 400 °C and crystallized above 600 °C. Chlorine atoms were not included in an as-deposited film. The film deposited in BTT solution grew maintaining a lower RMS value than the film deposited in the TC solution.

Acknowledgment. This work was supported by a Grant-in-Aid from the Japan Society for the Promotion of Science (JSPS).

LA026158+

(43) Wasserman, S. R.; Tao, Y.-T.; Whitesides, G. M. *Langmuir* **1989**, *5*, 1074.

(44) Kluth, G. J.; Sung, M. M.; Maboudian, R. *Langmuir* **1997**, *13*, 3775−3780.

(45) Phani, A. R.; Manorama, S.; Rao, V. J. *Mater. Chem. Phys.* **1999**, *58*, 101−108.

(46) Zhu, P. X.; Masuda, Y.; Koumoto, K. *J. Colloid Interface Sci.* **2001**, *243*, 31−36.